Indolepropionic acid modulates the immune response in allergic rhinitis through the AKT/CEBPB/IL-10 signaling pathway

LU GAO, YULAN SONG, FENGYAO ZHANG, YAN ZHAO, HUIXUAN HU and YAN FENG

Department of Otorhinolaryngology Head and Neck Surgery, The First Hospital of Shanxi Medical University, Taiyuan, Shanxi 030001, P.R. China

Received December 4, 2024; Accepted April 9, 2025

DOI: 10.3892/mmr.2025.13569

Abstract. Allergic rhinitis (AR) is a common inflammatory disorder of the nasal mucosa, usually triggered by environmental allergens. Indolepropionic acid (IPA) can influence immune responses; however, the specific mechanisms underlying the effects of IPA on immune regulation in AR remain largely unexplored. In the present study, an experimental mouse model of AR was established by sensitizing and exposing the mice to allergens, followed by the administration of IPA via gavage. Nasal symptoms were assessed through behavioral scoring, histological examinations were conducted to evaluate changes in nasal mucosa, and cytokine levels were quantified using ELISA. The expression of key signaling molecules was analyzed by immunohistochemistry, reverse transcription-quantitative PCR and western blotting. Additionally, the effects of IPA combined with an AKT inhibitor (HY-10355) on signaling pathway-related proteins in human nasal epithelial cells were evaluated using cellular immunofluorescence and western blotting. The results revealed that IPA treatment significantly reduced nasal inflammation, as indicated by decreased sneezing and mucus secretion. Histological analysis showed reduced inflammatory cell infiltration and epithelial damage in IPA-treated mice compared to controls. Furthermore, cytokine analysis revealed reduced levels of the pro-inflammatory cytokines IL-4, IL-5, IL-13 and immunoglobulin E, along with increased levels of the anti-inflammatory cytokine IL-10. Molecular investigations demonstrated that IPA can activate the AKT/CCAAT enhancer binding protein β pathway, leading to increased IL-10 expression and reduced inflammation. In conclusion, these findings suggested that IPA may serve as a promising therapeutic strategy for managing AR, pending further clinical validation.

Correspondence to: Professor Yan Feng, Department of Otorhinolaryngology Head and Neck Surgery, The First Hospital of Shanxi Medical University, 85 Jiefang South Road, Taiyuan, Shanxi 030001, P.R. China
E-mail: fengyan@sxmu.edu.cn

Key words: allergic rhinitis, indolepropionic acid, immune modulation, AKT/CCAAT enhancer binding protein β/IL-10 pathway, inflammatory response

Introduction

Allergic rhinitis (AR) is a non-infectious inflammatory condition of the nasal mucosa, which is driven by immunoglobulin E (IgE), and impacts 10-30% of the global population (1). When exposed to allergens, such as pollen, dust mites and pet dander, the immune system generates IgE antibodies that attach to mast cells, prompting the release of inflammatory mediators, including histamine. This cascade leads to nasal mucosal inflammation and distinct symptoms, such as nasal congestion, rhinorrhea, frequent sneezing and ocular discomfort (2).

The impact of AR extends beyond physical symptoms, significantly affecting quality of life through sleep disturbances, decreased work productivity and restricted social interactions (3). Additionally, individuals with AR face elevated risks of anxiety, depression and comorbid conditions, such as asthma (4,5). Despite its widespread prevalence, the treatment options for AR remain limited, with allergen-specific immunotherapy standing as the sole recognized cure. While this approach gradually diminishes allergen sensitivity, it underscores the pressing need for innovative therapeutic strategies (6).

Short-chain fatty acids (SCFAs) are synthesized by gut microbiota via dietary fiber fermentation. These SCFAs are pivotal for immune modulation and inflammation management, which are crucial in maintaining host well-being, particularly through their anti-inflammatory properties (6). Research has highlighted the significance of SCFAs in treating AR, since individuals with AR often exhibit an altered gut microbiota composition characterized by diminished SCFA-producing bacteria (7,8). This dysbiosis may increase susceptibility to and the severity of AR (9). Consequently, supplementation with SCFAs has emerged as a promising prevention and treatment strategy for AR. Indolepropionic acid (IPA), a derivative of SCFAs, has garnered considerable attention due to its notable anti-inflammatory and immunomodulatory abilities (10). IPA is synthesized by specific flora in the gut, such as *Clostridium* spp., via the tryptophan metabolic pathway. It not only possesses strong antioxidant properties, but also serves a crucial role in inflammatory regulation by activating the aryl hydrocarbon receptor (AhR) and modulating the function of

immune cells (11). Studies have shown that IPA effectively alleviates IL-1β-induced chondrocyte inflammation, and attenuates the toxicity of organophosphorus pesticide exposure to the liver and kidney through the AhR/NF-κB regulatory axis, as demonstrated by a significant decrease in pro-inflammatory cytokine levels (12,13). Our prior investigation demonstrated significantly lower serum propionic acid (PA) levels in patients with AR compared with those in healthy controls, alongside a declining trend in IL-10 levels (14). It was thus hypothesized that IPA, as a derivative of SCFAs, may have a similar function, i.e., the ability to elevate the levels of IL-10.

The AKT protein is pivotal in cell signaling across diverse cell types, and is closely associated with regulating immune responses and inflammation (15). CCAAT enhancer binding protein β (CEBPB) belongs to the CEBP family, which includes α-ζ members and is characterized by a conserved leucine zipper (bZIP) domain at its carboxyl terminus that aids in dimerization and DNA binding (16,17). CEBPB is widely expressed in various tissues and governs a range of biological processes, such as immune responses (18,19), aging (20) and the development of different types of cancer (21). In innate immune cells, CEBPB helps suppress the production of inflammatory cytokines while enhancing IL-10 expression (22). Notably, it has been demonstrated that increased CEBPB levels can enhance activation of the IL-10 promoter (23), serving a crucial role in IL-10 expression in macrophages (22). These findings suggest that IPA may mitigate the symptoms of AR by upregulating IL-10 levels through the AKT/CEBPB/IL-10 signaling pathway.

Despite exploring the immunomodulatory impacts of IPA and PA, its precise role in AR remains uncertain. The present study aimed to evaluate the therapeutic potential of IPA in alleviating AR symptoms with a mechanism that partially coincides with PA. The study also comprehensively investigated how IPA and PA mitigate the inflammatory response in AR via the AKT/CEBPB/IL-10 signaling pathway.

Materials and methods

Cells and reagents. Human nasal mucosal epithelial cells (HNEpCs) were purchased from Shanghai Huzhen Industrial Co., Ltd. at passage 4. IPA, PA and ovalbumin (OVA) were purchased from Sigma-Aldrich; Merck KGaA. The solvent used for the aluminum hydroxide solution was saline.

Establishment of a mouse model of AR. The experimental procedures followed the guidelines set by the Ethical Review Committee for Laboratory Animal Welfare of The First Hospital of Shanxi Medical University (approval no. DWLL-2024-015; Taiyuan, China). The experiment followed the Guide for the Care and Use of Laboratory Animals (24). Female BALB/c mice (n=30; weight, 20 g; age, 6-8 weeks) were obtained from Nanjing Junke Bioengineering Co., Ltd. The mice were housed in a controlled environment with a temperature of 25±1˚C and a relative humidity of 45-55%, under a 12-h light-dark cycle, with *ad libitum* access to food and water. Mice were thoroughly examined and observed twice daily at 8:30 a.m. and 5:30 p.m. to ensure that they received adequate attention and care during the experiment. Prior to the commencement of the experiment, the mice were acclimated for 1 week following standard procedures to ensure that they were familiar with and adapted to the new living environment. Subsequently, a 29-day experimental intervention phase was initiated. During this period, the mice were provided with ample feed and maintained a comfortable living environment to ensure the smooth progression of the experiment and data reliability. The entire experimental procedure, including the feeding adaptation period and the experimental intervention period, spanned a total of 36 days.

The literature relevant to OVA-sensitized mice was extensively reviewed (25,26) and our expertise was drawn upon in developing the mouse models of AR. The mice were randomly assigned to the following three groups: i) A blank control group (Control group), ii) an OVA sensitization group (OVA group) and iii) an IPA treatment group (OVA + IPA group). Sensitization involved intraperitoneal injections of OVA (100 μg/mouse in 0.1 ml 1 mg/ml aluminum hydroxide solution) on days 0, 7 and 14, followed by daily nasal administration of OVA (20 μl/nostril, 10 mg/ml) between days 21 and 28. The concentration of IPA and the intervention duration were established based on the preliminary investigation by Zhou *et al* (14) and our pre-experiment. The OVA + IPA group was also administered a daily oral gavage of IPA (20 mg/kg) throughout the same timeframe. The control group received saline injections and nasal stimulation. The volume of saline used for the control group during both the sensitization and challenge phases was identical to that used for the mice in the OVA group. Furthermore, during the nasal stimulation experiment, a pre-prepared OVA solution was employed. For the specific procedure, mice were placed in a comfortable position, and a 20-μl pipette was used to slowly administer the solution intranasally, to minimize the discomfort of the mice and prevent asphyxiation (Fig. 1). On the final day, after deeply anesthetizing the mice via intraperitoneal injection with 50 mg/kg sodium pentobarbital, the mice were euthanized by cervical dislocation, and nasal mucosa and blood samples were collected. Animal euthanasia was confirmed by observing respiration and heartbeat, examining pupil reactions and using the touch method, which specifically entailed checking the skin temperature by touching, and assessing heartbeat and pulse through palpation. Throughout the experiment, the health status of the mice was closely monitored and no unexpected deaths occurred. When the mice appeared to have seriously deteriorated in health, were untreatable or exhibited abnormal behavior, or when the purpose of the experiment had been achieved and no further valuable data could be obtained, the principles of the ethics review were strictly followed and the animals were euthanized. This was done to minimize the pain and discomfort suffered by the mice. No mice were sacrificed early due to the aforementioned circumstances. All mice died as a result of the euthanasia procedure required by the experimental design, in full compliance with ethical review requirements and animal welfare standards.

AR symptom scores. During the 21-28-day post-sensitization period, an observer blinded to the groupings recorded the frequency of sneezing and nose scratching, and the intensity of rhinorrhea in the mice. The symptoms were assessed using a standardized scale after OVA exposure, with a total score >5 indicating effective sensitization (27). The score for AR (SFAR)

Table I. Symptom scores of AR evaluation.

Symptom	Slight (1 point)	Moderate (2 points)	Severe (3 points)
Sneezing, times/30 min	1-3	4-10	>11
Nasal scratching, times/30 min	1-5	6-15	>15
Rhinorrhea	Flow to anterior nasal foramen	Beyond the anterior nasal foramen	Nasal discharge flowing onto the face

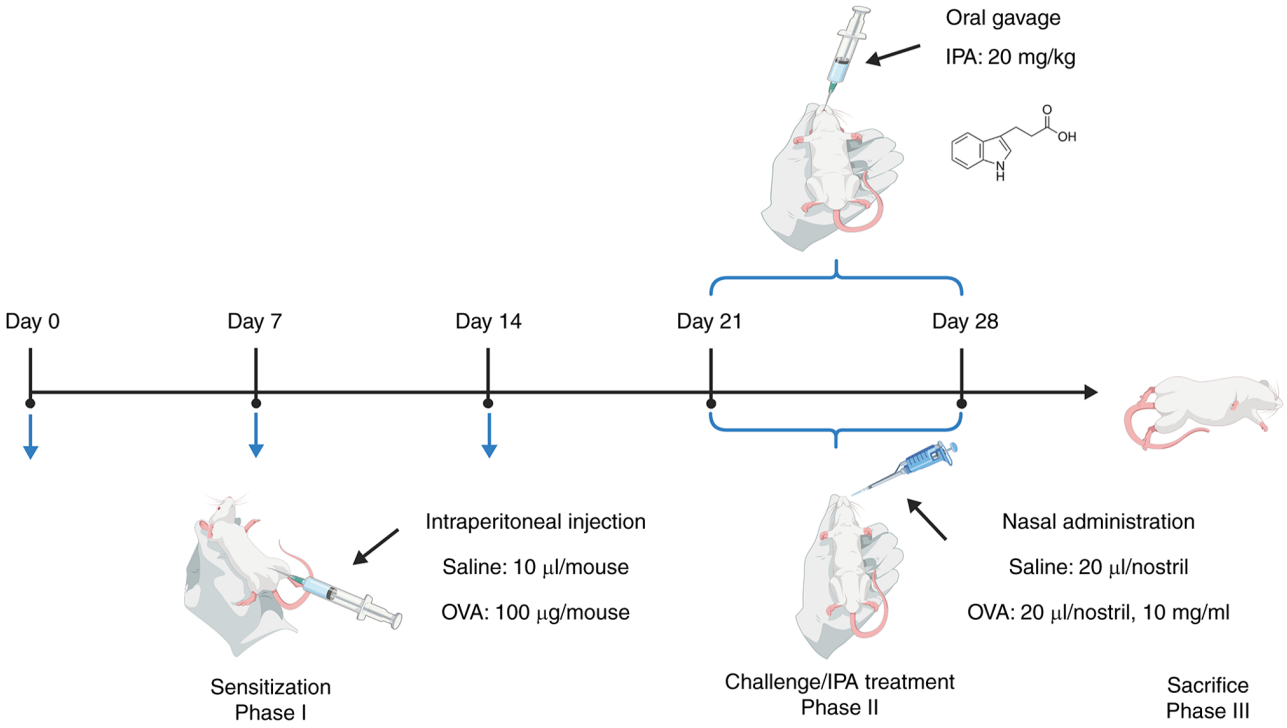

Figure 1. Procedure for sensitization and drug treatments. Image created using BioGDP.com. IPA, indolepropionic acid; OVA, ovalbumin.

was calculated as the sum of the scores for sneezing, nasal scratching and rhinorrhea; and the total scores were analyzed using a non-parametric test. The specific scoring details are summarized in Table I.

Histopathological examination of nasal mucosa. The mouse nasal mucosa epithelium was excised and fixed in 4% paraformaldehyde for 24 h at 4˚C. Following fixation, the samples underwent dehydration using a tissue dehydrator and were embedded in paraffin. Each paraffin-embedded block was pre-frozen at -20˚C for 30 min, sectioned to a thickness of 5 μm and then baked for 2 h. Subsequently, the sections were deparaffinized using xylene and ethanol gradients, and were subjected to hematoxylin and eosin (H&E) staining, periodic acid-Schiff staining (PAS) and toluidine blue staining (TBS).

H&E, PAS and TBS (1%) (cat. nos. G1120, G1281 and G3668; all from Beijing Solarbio Science & Technology Co., Ltd.), were used at their original concentrations as produced by the manufacturer. The staining procedures were performed at room temperature. For H&E staining, the sections were dewaxed in 100% xylene twice (10 min each), rehydrated through a graded series of ethanol (100, 95, 85 and 75%; 3 min each) and then immersed in distilled water for 2 min. After staining with hematoxylin solution for 5 min and rinsing with distilled water to remove excess stain, the sections were differentiated with differentiation solution for 30 sec, followed by two 5-min rinses with tap water. Eosin staining was then performed for 1 min, after which excess stain was removed and sections were rapidly dehydrated. For dehydration, clearing and mounting, sections were sequentially immersed in graded ethanol (75, 85, 95 and 100% ethanol, 3 sec each; 100% ethanol for 1 min; and 100% xylene twice, 1 min each), before being mounted with neutral gum.

For PAS, the sections were rinsed with tap water for 3 min and then with distilled water twice, before applying periodic acid and incubating the sections at room temperature for 5 min. After another rinse with tap water and two rinses with distilled water, Schiff staining solution was applied and the sections were stained in the dark for 10 min. After a 10-min rinse with distilled water, the sections were immersed in hematoxylin staining solution for 1 min to stain the nuclei, differentiated with acidic differentiation solution for 5 sec and then blued in tap water for 10 min. Finally, sections were dehydrated

through a graded series of ethanol, cleared in 100% xylene, and mounted with neutral gum.

For TBS, paraffin-embedded sections were dewaxed in 100% xylene twice (15 min each), rehydrated through a series of ethanol solutions (1 min each) and then rinsed with distilled water for 2 min. TBS solution was then applied for 10 min, followed by a 1-min rinse with distilled water and blotting dry with filter paper. Sections were differentiated with 95% ethanol until mast cells appeared purple-blue and the background light blue, rapidly dehydrated in 95% ethanol for 5 sec and then immersed in absolute ethanol twice (1 min each). Finally, the sections were cleared in 100% xylene and mounted with neutral gum. Pathological changes were examined under a light microscope (Pannoramic Scan II; 3DHISTECH, Ltd.) and image analysis was performed using CaseViewer 2.4.0 (https://www.lumingrj.com/2024/12/18/WIN/CaseViewer-2.4.0).

ELISA. Mouse blood was collected from the eyeballs of mice after sacrifice and incubated at room temperature for 2-3 h. The whole blood was centrifuged at 1,800 x g for 15 min at room temperature to obtain the serum. Subsequently, the levels of the inflammatory factors IL-4, IL-5, IL-10, IL-13 and IgE were quantified using ELISA-specific kits (cat. nos. JM-02448M1, JM-02447M1, JM-02459M1, JM-02456M1 and JM-02339M1, respectively; Jiangsu Jingmei Biological Technology Co., Ltd.) according to the manufacturer's protocol.

Immunohistochemistry staining. The immunohistochemical assay was employed to evaluate the expression levels of AKT, phosphorylated (P)-AKT, CEBPB and IL-10 in the epithelial tissues of the mouse nasal mucosa. Tissue sections underwent deparaffinization following H&E staining, followed by immersion in water for 10 min. Subsequently, the sections were treated with 0.01 M sodium citrate buffer (pH 6.0) and subjected to heat treatment in a pressure cooker. After the rotary valve popped up, which indicated that the water temperature had reached 100˚C, the sections were heated for 2 min and then cooled to room temperature naturally. Endogenous peroxidase activity was blocked using a freshly prepared 3% H_2O_2 methanol solution for 10 min in the dark at room temperature, and the sections were subsequently washed with PBS. The sections were then incubated with sheep-derived blocking serum (cat. no. ZLI-9022; Beijing Zhongshan Jinqiao Biotechnology Co., Ltd.) at room temperature for 20 min. Primary antibodies (AKT: Cat. no. 10176-2-AP, 1:100; P-AKT (Ser473): Cat. no. 66444-1-Ig, 1:100; CEBPB: Cat. no. 23431-1-AP, 1:100; IL-10: Cat. no. 60269-1-Ig, 1:100; all from Wuhan Sanying Biotechnology) were then used to incubate the sections overnight at 4˚C. On the following day, after the primary antibodies were removed, an appropriate quantity of secondary antibody (enzyme-labeled goat anti-mouse/rabbit IgG polymer: Cat. no. PV-6000, 1:100; Beijing Zhongshan Jinqiao Biotechnology Co., Ltd.) was applied, followed by color development using freshly prepared DAB solution (cat. no. ZLI-9017; Beijing Zhongshan Jinqiao Biotechnology Co., Ltd.). The reaction was halted with tap water post-color development, and counterstaining was performed at room temperature with hematoxylin staining solution for 1 min, followed by rinsing with tap water for 10 min to reverse the blue coloration. Finally, the slides were sealed with resin and images were captured using an optical microscope. Finally, randomly selected regions were analyzed using ImageJ-win64 software (National Institutes of Health) to determine the expression levels of the target proteins.

Table II. Primer sequences.

Gene	Primer sequence
AKT	F: 5'-GTGGCAGGATGTGTATGAGAAGAAG-3'
	R: 5'-AGGCGGCGTGATGGTGATC-3'(Reverse)
CEBPB	F: 5'-GCAATCCGGATCAAACGTGG-3'
	R: 5'-GATTACTCAGGGCCCGGCTG-3'
IL-10	F: 5'-GGACAACATACTGCTAACCGACTC-3'
	R: 5'-TGGATCATTTCCGATAAGGCTTGG-3'
IL-4	F: 5'-CCATATCCACGGATGCGACA-3'
	R: 5'-CGTTGCTGTGAGGACGTTTG-3'
IL-5	F: 5'-CCACATGCTGGGCCTTACTT-3'
	R: 5'-GTAAACTGGGGGAGGCTTCT-3'
IL-13	F: 5'-ATGGCCTCTGTAACCGCAAG-3'
	R: 5'-CTCATTAGAAGGGGCCGTGG-3'
GAPDH	F: 5'-GGTTGTCTCCTGCGACTTCA-3'
	R: 5'-TGGTCCAGGGTTTCTTACTCC-3'

CEBPB, CCAAT enhancer binding protein β.

Reverse transcription-quantitative PCR (RT-qPCR). The nasal mucosa tissue was removed from the -80˚C freezer and thawed, TriQuick (cat. no. R1100, Beijing Solarbio Science & Technology Co., Ltd.) was added and the tissue underwent lysis in a homogenizer. Subsequently, chloroform was added, and the sample was mixed and centrifuged at 12,000 x g for 15 min at 4˚C. The upper layer was then collected, mixed with isopropanol and incubated at -20˚C overnight. The next day, the RNA precipitate was obtained by centrifugation at 12,000 x g for 10 min at 4˚C, and RNA was reverse transcribed into cDNA using the RT kit (cat. no. RR036A; Takara Bio, Inc.) according to the manufacturer's instructions, as follows: 37˚C for 15 min, 85˚C for 15 sec and 16˚C indefinitely. Subsequently, qPCR was performed using 2X M5 HiPer SYBR Premix EsTaq (with Tli RNaseH) (cat. no. MF787-01; Mei5 Biotechnology, Co., Ltd). The thermocycling conditions were as follows: Pre-denaturation at 95˚C for 30 sec, followed by 40 cycles at 95˚C for 5 sec and 60˚C for 30 sec, and a final melt curve analysis. The relative mRNA expression levels were calculated using the $2^{-\Delta\Delta Cq}$ method (28) with GAPDH as an endogenous control. The primer sequences are listed in Table II.

HNEpC culture and intervention. HNEpCs were cultured in DMEM (Thermo Fisher Scientific, Inc.) supplemented with 5% fetal bovine serum (cat. no. SA301.02, Cellmax Co., Ltd.) and 1% penicillin/streptomycin solution) (cat. no. PWL062; Dalian Meilun Biology Technology Co., Ltd.) at 37˚C in a humidified atmosphere containing 5% CO_2. Upon reaching 80% confluence, the cells were passaged and seeded into 6-well plates. All groups were treated at 37˚C in a humidified atmosphere containing 5% CO_2. The cells were then divided

into four groups for treatment: Control group received standard medium as a control; OVA group was exposed to 0.1% OVA (dissolved in standard medium) for 24 h; OVA + PA group was treated with 20 μmol/l PA (dissolved in standard medium) for 24 h following 24 h of intervention with 0.1% OVA; and OVA + PA + AKT inhibitor VIII group was pretreated with 10 mmol/l AKT inhibitor VIII (cat. no. HY-10355; MedChemExpress) (dissolved in DMSO) for 5 h before the addition of 0.1% OVA for 24 h, followed by treatment with 20 μmol/l PA (dissolved in standard medium) for 24 h. The proteins were extracted at the end of the experiment and were subsequently subjected to western blot analysis to detect related markers.

Immunofluorescence staining. HNEpCs were cultured on sterile coverslips in 12-well plates until reaching 50% confluence and were treated as aforementioned. Following fixation with 4% paraformaldehyde for 10 min at room temperature, the coverslips were subjected to immunofluorescence staining. The harvested cells were permeabilized using a 1% Triton X-100 solution (cat. no. T8200; Beijing Solarbio Science & Technology Co., Ltd.) and antigenic blocking was carried out using sheep-derived blocking serum (cat. no. ZLI-9022; Beijing Zhongshan Jinqiao Biotechnology Co., Ltd.) at room temperature for 30 min. The cells were then incubated overnight at 4˚C with primary antibodies against AKT (cat. no. 10176-2-AP, 1:100), P-AKT (Ser473) (cat. no. 66444-1-Ig, 1:100), CEBPB (cat. no. 23431-1-AP, 1:100) and IL-10 (cat. no. 60269-1-Ig, 1:100) (all from Wuhan Sanying Biotechnology). Subsequently, the samples were incubated with the following secondary antibodies: CY3-conjugated avidin (cat. no. BA1037, 1:200) and DyLight® 488-conjugated avidin (cat. no. BA1128, 1:200) (both from Boster Biological Technology), for 1 h at room temperature in the dark. After staining with DAPI solution (cat. no. AR1176; 1:000; Boster Biological Technology) for 10 min at room temperature and washing with PBS three times (2 min/wash), anti-fluorescence quencher (cat. no. AR0036; Boster Biological Technology) was applied to the slides. The immunofluorescence slides were carefully removed from the well plates and incubated overnight at 4˚C prior to observation of the results using a fluorescence microscope. The fluorescence microscope revealed DAPI-labeled nuclei in blue, DyLight 488-labeled proteins in green and CY3-labeled proteins in red.

Western blot analysis. Total proteins were extracted from mouse nasal mucosa tissues and HNEpCs using RIPA lysis buffer (cat. no. AR0102; Boster Biological Technology), and the total protein concentration was quantified using a BCA kit (cat. no. AR1189; Boster Biological Technology) according to the manufacturer's instructions. The protein samples were then normalized, treated with 5X SDS-PAGE loading buffer and denatured at 100˚C for 10 min. Subsequently, the denatured proteins were separated by SDS-PAGE on a 10% gel and transferred to a PVDF membrane within 1.5 h. The PVDF membrane was blocked with 5% skim milk powder at room temperature for 2 h. Primary antibodies specific to AKT (cat. no. 10176-2-AP, 1:4,000), P-AKT (Ser473) (cat. no. 66444-1-Ig, 1:1,000), CEBPB (cat. no. 23431-1-AP, 1:6,000), IL-10 (cat. no. 60269-1-Ig, 1:4,000) and β-actin (cat. no. P60709, 1:10,000) from (all from Wuhan Sanying Biotechnology) were used to incubate the membranes overnight at 4˚C. After washing the membrane with TBS-0.1% Tween, the membranes were incubated for 2 h at room temperature with HRP-goat anti-rabbit IgG (cat. no. AS014; 1:10,000; ABclonal Biological Technology) and HRP-goat anti-mouse IgG (cat. no. BA1050; 1:10,000; Boster Biological Technology), before proceeding with further washing steps. Finally, protein signals on the membranes were detected using an ultrasensitive ECL chemiluminescence kit (cat. no. AR1171; Boster Biological Technology), and protein analysis was performed based on optical density measurements using ImageJ-win64 software.

Table III. Score of nasal symptoms.

Day	Control	OVA	OVA + IPA
Day 21	1.0 (1.0)	2.0 (1.0)	2.0 (1.0)
Day 22	2.0 (1.0)	3.0 (1.0)	3.5 (1.0)
Day 23	2.0 (1.0)	5.0 (2.0)	5.0 (2.0)
Day 24	2.0 (1.0)	5.5 (2.0)	5.0 (1.0)
Day 25	2.0 (1.0)	6.0 (2.0)	5.0 (0.5)
Day 26	2.5 (1.0)	7.0 (2.0)	5.5 (1.0)
Day 27	3.0 (0.5)	7.0 (1.0)	6.0 (1.0)
Day 28	3.0 (1.0)	9.0 (1.0)	6.0 (1.0)

Data are presented as median (IQR). IPA, indolepropionic acid; OVA, ovalbumin.

Statistical analysis. Data analysis was performed using GraphPad Prism 8.0 (Dotmatics). Data are presented as the mean ± standard deviation and were obtained from at least three independent experiments. For comparisons involving more than two groups, a one-way analysis of variance was performed, followed by Tukey's multiple comparisons test to evaluate pairwise distinctions. The non-parametric Kruskal-Wallis test and Dunn's post hoc test was employed to analyze the SFAR and rhinorrhea score, and these data are presented as the median (IQR). $P<0.05$ was considered to indicate a statistically significant difference.

Results

Behavioral scores of AR model mice. On day 21 of sensitization, mice in the OVA group began showing visible signs of sneezing, nose scratching and rhinorrhea, with symptoms escalating as OVA stimulation increased. Analysis of behavioral recordings revealed that by day 8 of stimulation, scores for the blank control group remained <5, in contrast to the OVA group, where scores for nasal symptoms >5, confirming the successful model construction (Table III). Furthermore, mice in the OVA + IPA group exhibited a gradual alleviation of AR symptoms upon IPA drug intervention, with statistical significance ($P<0.05$) observed from day 5 onwards (Fig. 2A). By the final day of stimulation, significant reductions in sneezing, nose scratching and rhinorrhea symptoms were evident in the OVA + IPA group, with behavioral scores for nasal symptoms

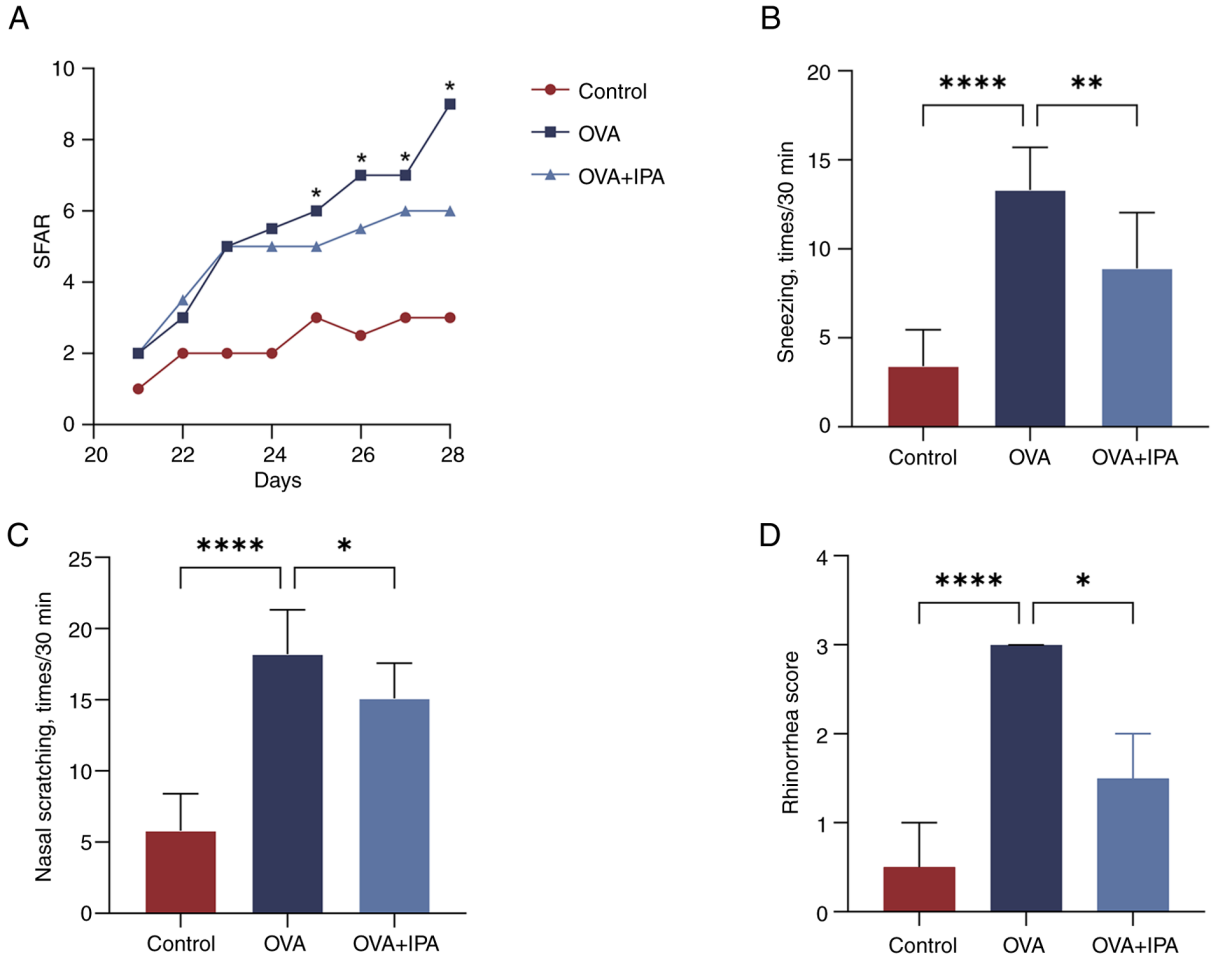

Figure 2. Behavioral scores of nasal symptoms. (A) Comparison of behavioral scores of nasal symptoms in mice. Comparison of (B) sneezing and (C) nasal scratching in each group on the last day of OVA stimulation. (D) Comparison of rhinorrhoea score in each group on the last day of OVA stimulation. Data are presented as the mean ± standard deviation, n=10 mice/group. *P<0.05, **P<0.01, ****P<0.0001 vs. OVA + IPA or as indicated. IPA, indolepropionic acid; OVA, ovalbumin; SFAR, score for allergic rhinitis.

significantly decreased compared with those in the OVA group (P<0.05; Fig. 2B-D).

Pathologic changes of nasal mucosa in AR model mice after IPA intervention. Histological examination using H&E staining revealed that the nasal mucosal epithelium in the control group exhibited structural integrity with uniformly arranged cilia, smooth submucosal blood vessels and the absence of scattered inflammatory cells (Fig. 3A). By contrast, the OVA group showed discontinuous and disorganized nasal mucosal epithelium, infiltration of numerous inflammatory cells, mucosal edema, congested and dilated arteriolar blood vessels, and varying degrees of nasal mucosa detachment. PAS and TBS staining indicated the presence of proliferating cup cells and mast cells in the OVA group, with cup cells stained purple-red and mast cells stained purple (Fig. 3B and C). Treatment with IPA resulted in a reduction in the aforementioned cell number of cup cells and mast cells.

Alterations in serum inflammatory cytokines in AR model mice after IPA intervention. The levels of cellular inflammatory factors (IL-4, IL-5, IL-13, IgE and IL-10) were detected in mouse serum samples using ELISA. Significantly higher levels of IL-4, IL-5, IL-13 and IgE were observed in the OVA group compared with those in the Control and OVA + IPA groups (P<0.05; Fig. 4A, B, D and E). Conversely, IL-10 levels were significantly higher in the Control and OVA + IPA groups than those in the OVA group (P<0.05; Fig. 4C).

Alterations in the AKT/CEBPB/IL-10 signaling pathway after IPA intervention. The immunohistochemical analysis of AKT, P-AKT, CEBPB and IL-10 expression in mouse nasal mucosa tissues was conducted using a light microscope and analyzed with ImageJ software (Fig. 5). AKT and P-AKT were observed in the nucleus and cytoplasm; CEBPB was predominantly nuclear; and IL-10 was detected in the nucleus, cytoplasm and extracellularly, with positive staining appearing brownish-yellow (Fig. 5A). Significantly lower levels of P-AKT and IL-10 were detected in the OVA group compared with those in the Control group (P<0.05; Fig. 5C, D and F). Conversely, the OVA + IPA group exhibited significantly increased expression levels of P-AKT, CEBPB and IL-10 compared with those in the OVA group (P<0.05; Fig. 5B-F).

Changes in the expression levels of genes in the inflammatory signaling pathway. Based on the immunohistochemical findings, RT-qPCR was utilized to assess the mRNA expression levels of AKT, CEBPB, IL-10, IL-4, IL-5 and IL-13 in the nasal

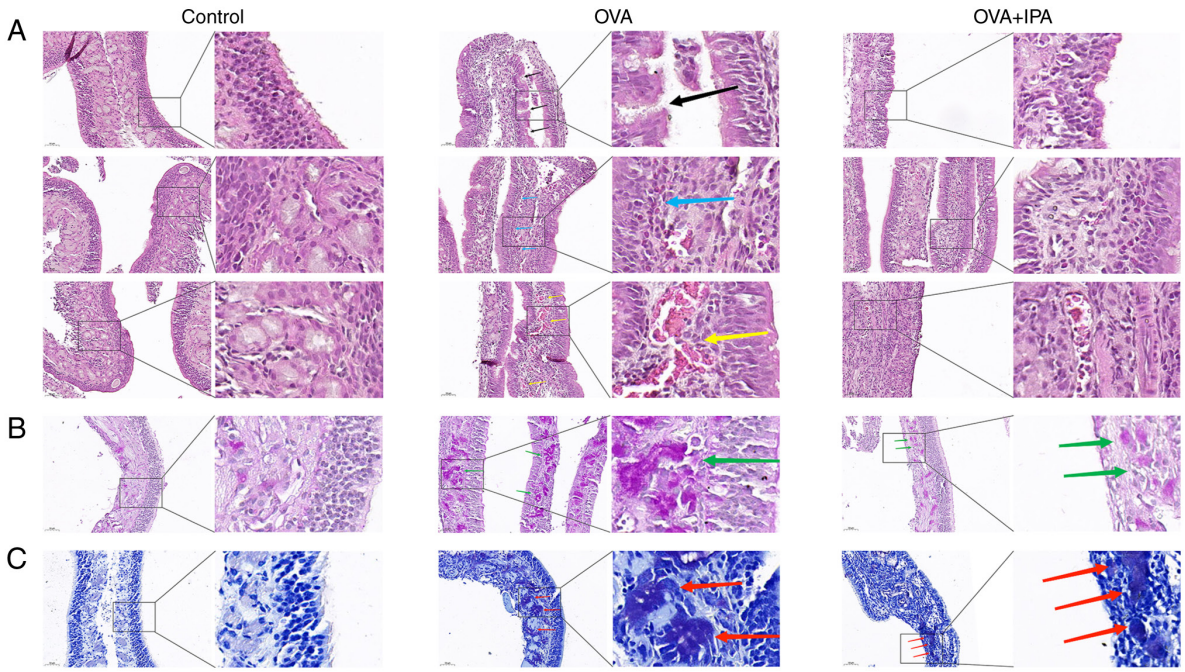

Figure 3. Pathological changes of nasal mucosa in IPA-treated mice with allergic rhinitis. (A) Hematoxylin and eosin staining (magnification in the smaller images, x20) was used to observe the histopathological changes of the nasal mucosal epithelium. The black arrow indicates mucosal epithelium destroyed and damaged, the blue arrow indicates eosinophil infiltration and the yellow arrow indicates vascular congestion and diastole of small arteries. (B) Periodic acid-Schiff staining (magnification in the smaller images, x20) was used to observe the cup cells of the nasal mucosa (green arrows). (C) Toluidine blue staining (magnification in the smaller images, x20) was used to observe the mast cells of the nasal mucosa (red arrows). IPA, indolepropionic acid; OVA, ovalbumin.

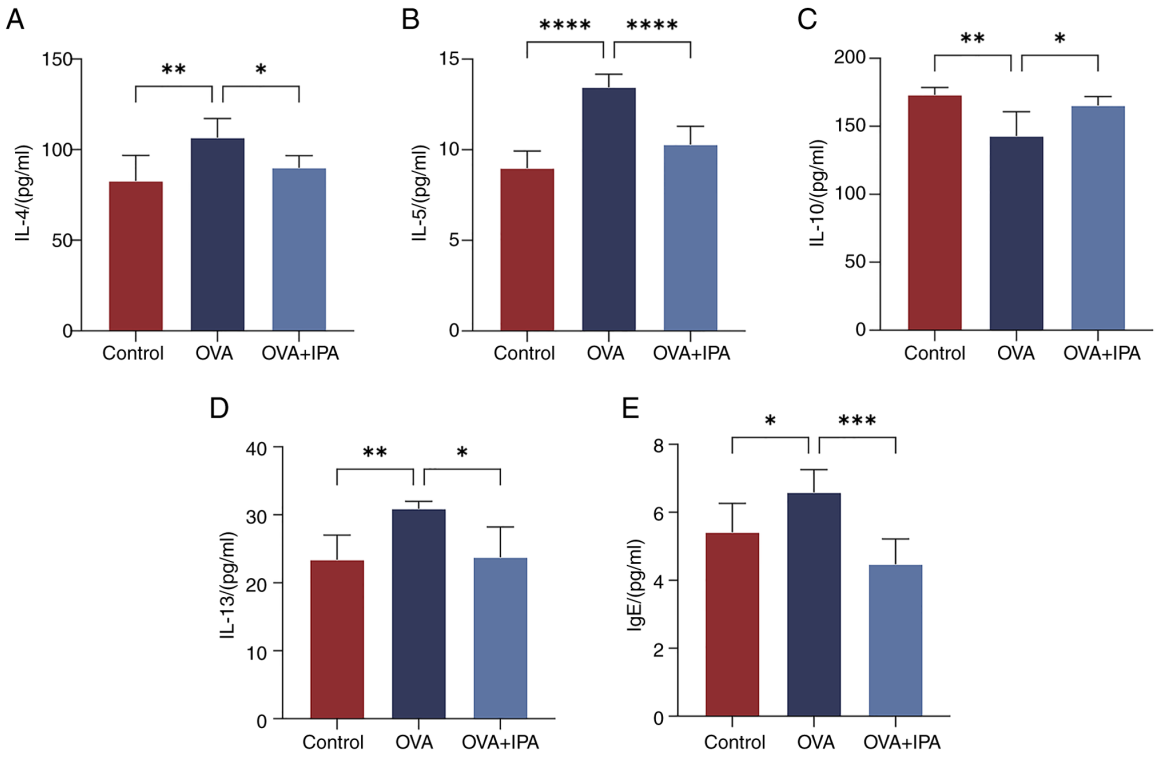

Figure 4. Changes in serum inflammatory cytokines in allergic rhinitis model mice following treatment with IPA. Serum levels of (A) IL-4, (B) IL-5, (C) IL-10, (D) IL-13 and (E) IgE were measured by ELISA. Data are presented as the mean ± standard deviation, n=6. *P<0.05, **P<0.01, ***P<0.001, ****P<0.0001. IgE, immunoglobulin E; IPA, indolepropionic acid; OVA, ovalbumin.

mucosa of mice across different experimental groups (Fig. 6). Statistical analysis revealed no significant differences in AKT levels among the various groups (P>0.05; Fig. 6A). Compared with those in the Control group, the OVA group exhibited notably decreased mRNA expression levels of CEBPB and IL-10, while showing significantly elevated levels of IL-4, IL-5

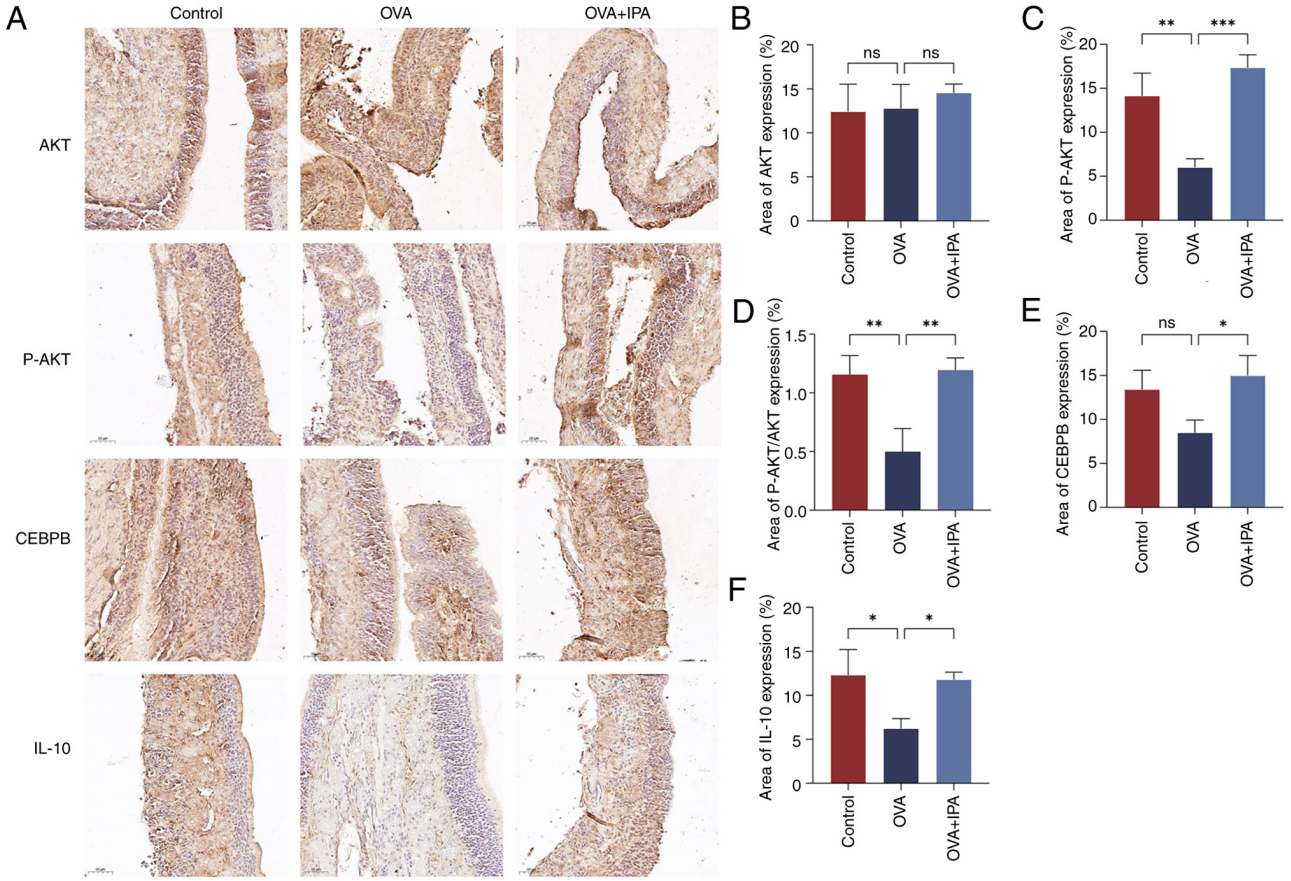

Figure 5. Alterations in the AKT/CEBPB/IL-10 signaling pathway after IPA intervention. (A) Immunohistochemistry staining results. Expression levels of (B) AKT, (C) P-AKT, (D) P-AKT/AKT, (E) CEBPB and (F) IL-10. Area (%) indicates the integrated optical density of the image/area. Data are presented as the mean ± standard deviation, n=3. *P<0.05, **P<0.01, ***P<0.001. CEBPB, CCAAT enhancer binding protein β; IPA, indolepropionic acid; ns, not significant; OVA, ovalbumin; P-, phosphorylated.

and IL-13 mRNA (P<0.05; Fig. 6B-F). Conversely, in contrast to the OVA group, the OVA + IPA group demonstrated significantly increased mRNA expression levels of CEBPB and IL-10, and significantly reduced levels of IL-4, IL-5 and IL-13 mRNA (P<0.05; Fig. 6B-F).

Changes in the expression levels of proteins in the inflammatory signaling pathway. The protein expression levels of AKT, P-AKT, CEBPB and IL-10 in the nasal mucosa of mice from each group were assessed using western blotting (Fig. 7). Compared with those in the Control group, the OVA group exhibited a significant decrease in the protein expression levels of CEBPB and IL-10 (P<0.05; Fig. 7E and F). Conversely, the OVA + IPA group displayed notably elevated protein expression levels of P-AKT, CEBPB and IL-10 compared with those in the OVA group (P<0.05; Fig. 7C-F).

Effect of inhibition of the AKT/CEBPB/IL-10 signaling pathway by AKT inhibitor VIII. To elucidate the impact of PA on AR via the AKT/CEBPB/IL-10 signaling pathway, HNEpCs were treated with AKT inhibitor VIII, OVA and PA, followed by western blot analysis (Fig. 8). The findings revealed a significant decrease in the protein expression level of CEBPB in the OVA group compared with the control group, and a significant increase in the protein expression levels of P-AKT, CEBPB and IL-10 in the OVA + PA group compared with those in the OVA group (P<0.05; Fig. 8C-F). Conversely, following AKT inhibitor VIII intervention, there was a notable decrease in the protein expression levels of P-AKT, CEBPB and IL-10 (P<0.05).

Effects of cotreatment with AKT inhibitor VIII, OVA and PA on the AKT/CEBPB/IL-10 signaling pathway. Immunofluorescence staining was utilized to detect the protein expression levels of AKT, P-AKT, CEBPB and IL-10 in the nucleus and cytoplasm (Fig. 9). Significantly decreased fluorescence staining signals of P-AKT, CEBPB and IL-10 were observed in the HNEpCs of the OVA group compared with those in the control group, whereas significantly increased fluorescence staining signals of P-AKT, CEBPB and IL-10 were observed in the HNEpCs of the OVA + PA group compared with those in the OVA group (P<0.05; Fig. 9F-I). Conversely, intervention with AKT inhibitor VIII led to a notable decrease in the fluorescence signals of P-AKT, CEBPB and IL-10 (P<0.05).

Discussion

AR, a common allergic condition, disrupts immune homeostasis by altering the T helper (Th)1/Th2 cell balance (29). Upon exposure to allergens, there is a predominance of Th2 cells that release cytokines, such as IL-4, IL-5 and

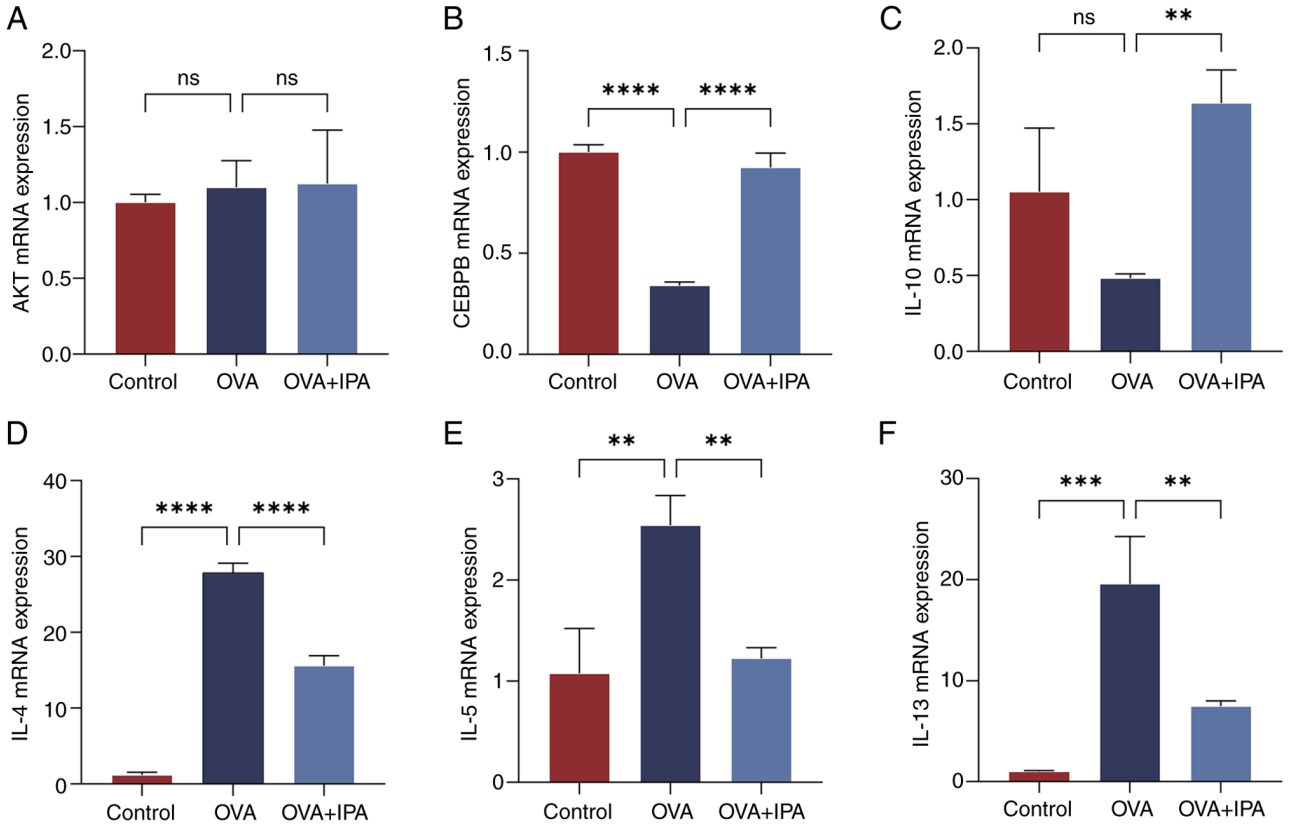

Figure 6. Changes in the expression levels in genes in the inflammatory signaling pathway. Comparison of the mRNA expression levels of the inflammatory signaling pathway factors (A) AKT, (B) CEBPB, (C) IL-10, (D) IL-4, (E) IL-5 and (F) IL-13 in mous nasal mucosal epithelial tissues across different groups. Data are presented as the mean ± standard deviation, n=3. **P<0.01, ***P<0.001, ****P<0.0001. CEBPB, CCAAT enhancer binding protein β; IPA, indolepropionic acid; ns, not significant; OVA, ovalbumin.

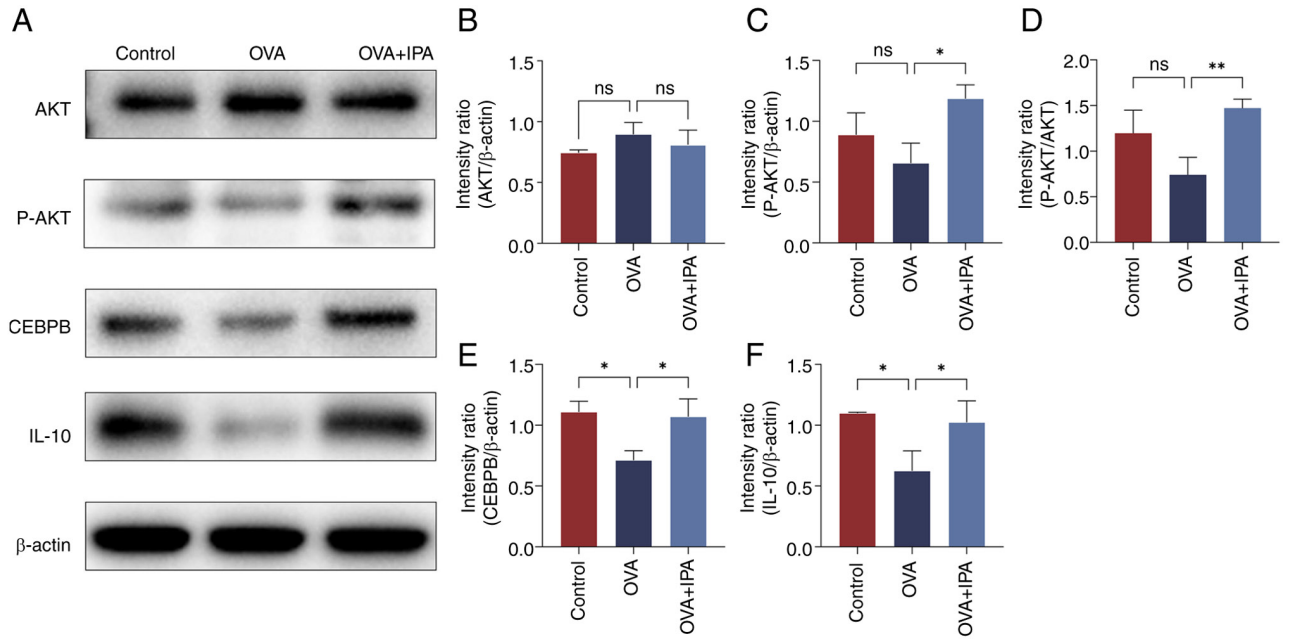

Figure 7. Changes in the expression levels in proteins in the inflammatory signaling pathway. (A) Western blot analysis of (B) AKT, (C) P-AKT, (D) P-AKT/AKT, (E) CEBPB and (F) IL-10 protein levels. Data are presented as the mean ± standard deviation, n=3. *P<0.05, **P<0.01. CEBPB, CCAAT enhancer binding protein β; IPA, indolepropionic acid; ns, not significant; OVA, ovalbumin; P-, phosphorylated.

IL-13, thus stimulating IgE production, eosinophil activation and mucus secretion (30). The sensitization to OVA imitates the typical pathological features observed in human AR, including IgE-mediated tachyphylaxis, eosinophilic

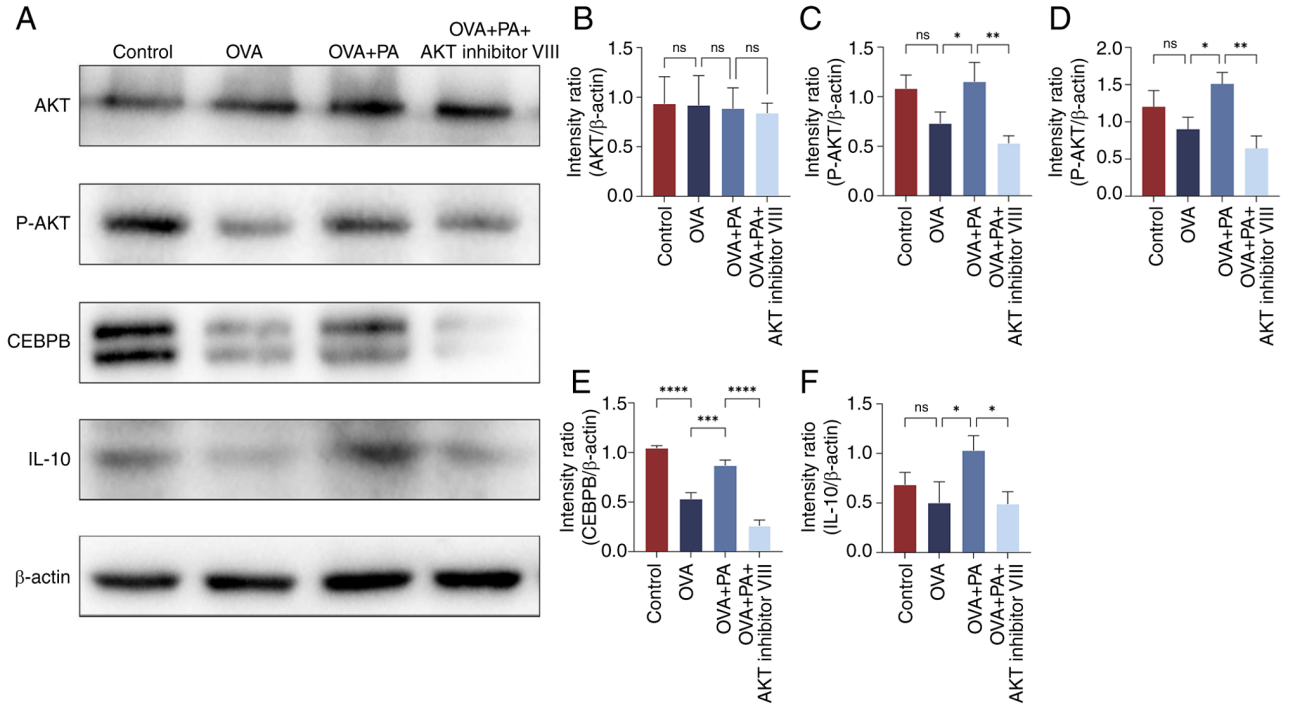

Figure 8. Protein expression levels of AKT, P-AKT, CEBPB and IL-10 in human nasal mucosal epithelial cells treated with AKT inhibitor VIII, OVA and PA. (A) Western blot analysis of (B) AKT, (C) P-AKT, (D) P-AKT/AKT, (E) CEBPB and (F) IL-10 protein levels. Data are presented as the mean ± standard deviation, n=3. *P<0.05, **P<0.01, ***P<0.001, ****P<0.0001. CEBPB, CCAAT enhancer binding protein β; ns, not significant; OVA, ovalbumin; P-, phosphorylated; PA, propionic acid.

infiltration, heightened Th2 cytokines (IL-4, IL-5, IL-13) and nasal mucosal edema (27,31,32). Our previous study further confirmed the typical representativeness of OVA in inducing AR in a mouse model by comparing the sensitizing properties of OVA with *Artemisia* pollen. Therefore, the OVA model was selected because it can accurately reflect the physiological and immune response characteristics of human AR (27). The current study established an AR mouse model using OVA, leading to pronounced symptoms. Histological examination demonstrated notable nasal mucosal damage characterized by vascular congestion and inflammatory cell infiltration, consistent with prior research (27). Significantly, these pathological changes were markedly alleviated with the administration of IPA treatment.

There is a growing interest in microbial metabolites, particularly SCFAs and their derivatives, for the modulation of the immune response (33). IPA is a microbial metabolite produced by gut bacteria through tryptophan decarboxylation, facilitated by specific strains such as *Clostridium perfringens* (34). Unlike PA derived directly from dietary fiber fermentation, IPA is a secondary metabolite linking tryptophan breakdown to SCFAs-related pathways (35). Recent studies have indicated that IPA possesses anti-inflammatory properties by influencing immune cell function, enhancing epithelial barrier integrity and regulating oxidative stress (36,37). Experimental evidence has demonstrated that IPA can alleviate inflammatory damage in human chondrocytes and colonic epithelial cells by modulating the NF-κB signaling pathway (12,38). These effects align with the reduced inflammation in AR observed in the present study, where IPA treatment significantly suppressed Th2 cytokines and increased IL-10 levels. Despite structural distinctions between PA and IPA, they exhibit similar immunomodulatory effects. PA primarily activates G-protein-coupled receptors, such as GPR41 and GPR43 (39). Our prior research suggested that GPR41 and GPR43 serve as upstream targets for PA, indirectly controlling the AKT pathway, which subsequently regulates IL-10 expression (14). GPR43 specifically mediates PA-induced IL-10 regulation in B cells. While the interaction of IPA with specific G-protein-coupled receptors remains less understood, it is conceivable that IPA may interact with these receptors through structural or functional mechanisms. Nonetheless, further experimental validation is required to verify this hypothesis.

In the present study, IPA exhibited a comparable capacity to activate the AKT/CEBPB/IL-10 signaling pathway to PA, indicating a convergence in their downstream effects. The distinct indole structure of IPA implies potential supplementary regulatory roles, such as influencing AhR-dependent gene expression (11,40), which may augment IL-10 production in B cells and macrophages. PA and IPA, which are predominantly synthesized by the gut microbiota, are subject to dietary and microbial influences. Dysbiosis in the gut microbiota of patients with AR, resulting in the diminished production of SCFAs, including IPA, could exacerbate allergic inflammation. In the present study, supplementation with IPA was shown to normalize IL-10 levels and mitigate inflammation, suggesting a compensatory function for IPA in the context of PA deficiency in AR. Moreover, IPA can facilitate PA synthesis by intestinal bacteria, with PA reciprocally impeding the degradation of IL-10 mRNA in regulatory B cells (Bregs) via the AKT/T-bet pathway; this stabilization of IL-10 expression in Bregs has been reported to effectively alleviate AR symptoms (14). Due

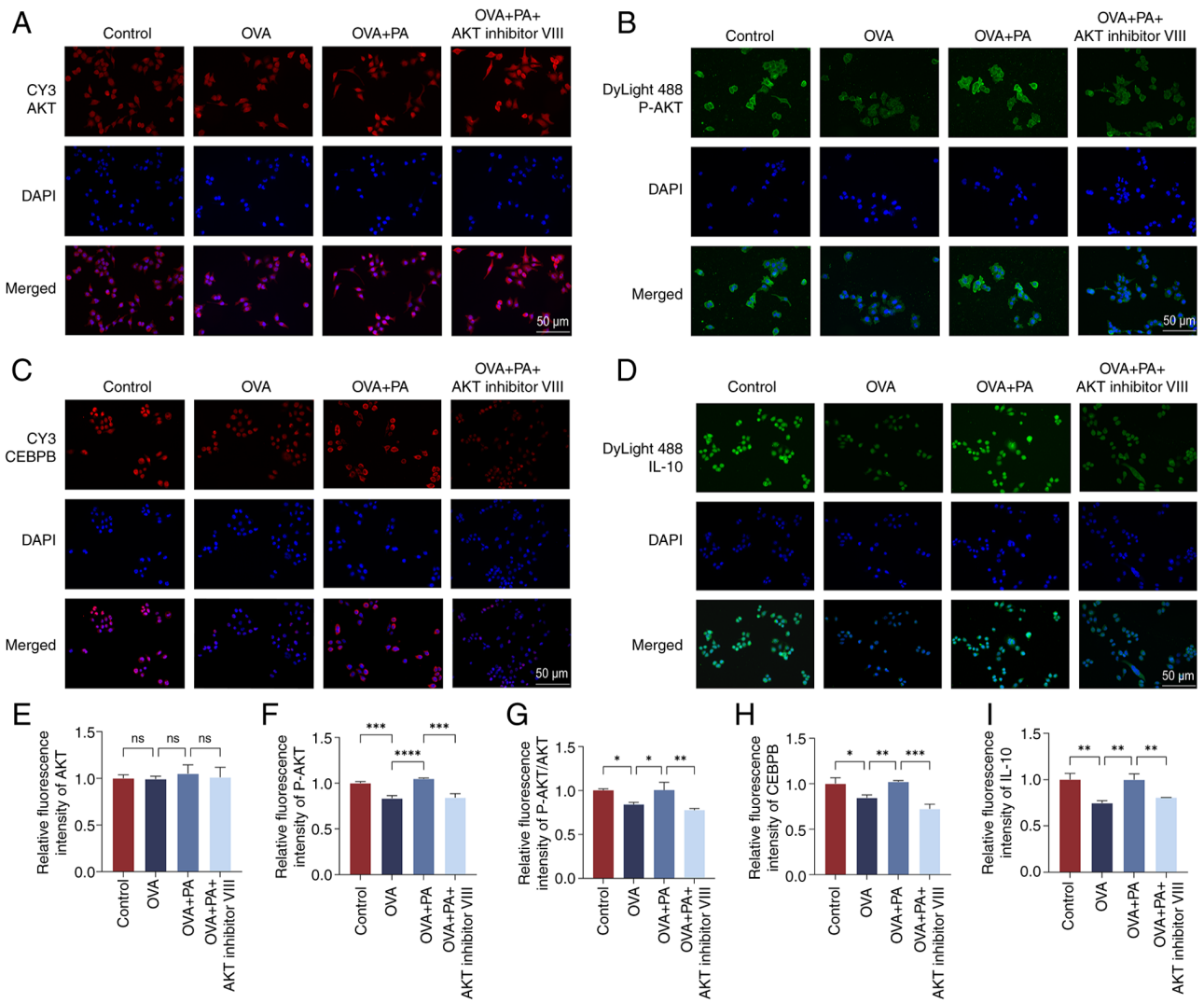

Figure 9. Localization and expression levels of AKT, P-AKT, CEBPB and IL-10 proteins in human nasal mucosal epithelial cells. Cellular immunofluorescence staining of (A) AKT, (B) P-AKT, (C) CEBPB and (D) IL-10. Relative fluorescence intensities of (E) AKT, (F) P-AKT, (G) P-AKT/AKT, (H) CEBPB and (I) IL-10. Data are presented as the mean ± standard deviation, n=3. *P<0.05, **P<0.01, ***P<0.001, ****P<0.0001. CEBPB, CCAAT enhancer binding protein β; ns, not significant; OVA, ovalbumin; P-, phosphorylated; PA, propionic acid.

to limitations, the changes in Tregs or B cells after IPA treatment were not evaluated in the present study. In the future, we aim to conduct relevant studies to assess the changes of these cells after IPA treatment; through this in-depth investigation, we aim to further confirm the central role of IL-10 in AR immunomodulation, and provide a more solid scientific basis and innovative ideas for the treatment and prevention of AR.

IL-10, a pivotal cytokine, is essential for maintaining immune homeostasis (41). In allergic conditions, Bregs and M2 macrophages can promote regulatory T-cell differentiation or directly inhibit T-cell proliferation by producing IL-10 and transforming growth factor β, thus restoring the balance between Th1 and Th2 cells, and reducing inflammation (42). IL-10 attenuates the activation of Th2 cells by inhibiting the expression of MHC-II molecules and co-stimulatory molecules on antigen-presenting cells, thereby suppressing their function (43). In addition, IL-10 exerts a positive regulatory effect on STAT3 by enhancing the phosphorylation of STAT3 in Th2 cells, which contributes to the reduction of inflammatory cytokine expression (IL-4, IL-5 and IL-13) in these cells (44). Moreover, inflammatory cytokines, such as IL-4 and IL-13, rapidly induce IL-10 production via STAT6 activation, a mechanism that effectively prevents excessive inflammatory responses (45,46). In the present study, the AKT/CEBPB/IL-10 signaling pathway was investigated, focusing on changes in IL-10 expression. The findings revealed a significant association between IL-10 expression and AR, with the OVA group exhibiting lower IL-10 levels than the other experimental groups. To understand the process by which IPA alleviates inflammation associated with AR by restoring the Th1/Th2 balance, IL-4, IL-5, IL-10 and IL-13 levels were also examined in the nasal mucosa and serum. However, the effects of IL-10 on these cytokines were not evaluated. ELISA detected increased levels of IL-4, IL-5, IL-13 and IgE in the serum of OVA-treated mice. Furthermore, the results of RT-qPCR confirmed the elevated expression of Th2 cytokines in the nasal mucosa post-OVA intervention, which was significantly reduced after IPA intervention. These findings may advance the understanding of the role of IL-10 in AR and suggest novel directions for future research.

CEBPB, a transcriptional regulator, serves a role in modulating immune and inflammatory responses (47,48). Its deficiency has been associated with excessive CD4 T-cell proliferation and the impaired function of regulatory T cells in colitis (49). Notably, SCFAs have been shown to down-regulate DUSP6 expression via the CEBPB/microRNA-145 pathway, reducing intestinal inflammation (50). In the present investigation, a notable difference was observed: CEBPB displayed a distinct single band in the western blot analysis of animal protein samples, whereas it exhibited double bands in cell protein samples. A comprehensive analysis led to the proposal that this variation could be attributed to disparities in processing and extraction methodologies, antibody specificity, post-translational protein modifications. and differences in sample concentrations between animal and cellular protein samples. In addition, the animal protein samples were derived from mouse mucosal epithelial tissue, whereas the cell protein samples were obtained human nasal mucosal epithelial cells; therefore, this different may also due to species-specific differences.

AKT is a key player in immune regulation, and the PI3K/AKT signaling pathway in dendritic cells has been shown to suppress inflammatory responses by increasing the expression of the anti-inflammatory cytokine IL-10 and decreasing the expression of the pro-inflammatory cytokine IL-12 (51). In the current study, a significant decrease in the expression levels of the pathway factors P-AKT, CEBPB and IL-10 were detected in the nasal mucosal epithelial tissues of mice with AR. Following intervention with IPA, these expression levels were significantly enhanced in AR model mice. Furthermore, intervention of OVA-sensitized HNEpCs with PA resulted in increased expression of P-AKT, CEBPB and IL-10 proteins. Conversely, inhibition of AKT led to a decrease in the expression levels of these molecules. These findings confirmed the pivotal role of PA and IPA in the pathogenesis of AR through the AKT/CEBPB/IL-10 signaling pathway.

Notably, it is essential to recognize the limitations of the present study. Firstly, it utilized a mouse model with OVA induction, mimicking key aspects of AR. However, caution is required when extrapolating the findings to humans without additional clinical validation. Secondly, using 16S rRNA sequencing and metabolomics analysis (52,53), previous studies have demonstrated that the gut microbiota can modulate immune responses by mediating IPA production. A previous comparison of microbiota profiles between patients with AR and healthy controls identified 37 bacterial taxa enriched in the healthy group, suggesting a potential role of microbiota changes in AR development (53). Although IPA, which is primarily produced by the gut microbiota, likely influences AR, the present study did not directly explore the specific contribution of the microbiota to IPA-mediated immune modulation. Future investigations, including 16S rRNA sequencing and metabolomics analyses, are planned to elucidate this relationship. Moreover, while IPA and PA share biological activities, there is inadequate evidence to support the complete substitution of PA with IPA. Further comprehensive studies are essential to fully comprehend the specific mechanisms and potential interchangeability between IPA and PA. Upon reviewing the experimental design of the present study, the absence of an OVA + AKT inhibitor VIII group constitutes an oversight. To enhance the rigor and completeness of the experiment, an OVA + AKT inhibitor VIII group will be included in future experiments, thereby further consolidating the scientific validity and reliability of the findings. Finally, the failure to consider concentration gradient modeling is another shortcoming of the current study, as it is critical for accurately assessing drug effects. In light of this, the incorporation of concentration gradient factors will be prioritized in our subsequent trial design.

In conclusion, IPA has emerged as a potential therapeutic option for AR by utilizing mechanisms similar to PA, including AKT/CEBPB/IL-10 activation, and by inducing unique immunomodulatory pathways associated with its indole structure. Future investigations should focus on exploring the combined utilization of IPA and PA, and their translational prospects in developing novel strategies for reinstating immune balance in allergic disorders.

Acknowledgements

Not applicable.

Funding

The present research project was supported by the Shanxi Scholarship Council of China (grant no. 2022-194) and the Fundamental Research Program of Shanxi Province (grant no. 202303021221218).

Availability of data and materials

The data generated in the present study may be requested from the corresponding author.

Authors' contributions

LG designed the research and wrote the draft. YS and FZ analyzed the experimental data. YZ and HH recorded animal behavior and provided data. YF participated in the conception and design of the research, provided resources and supervised the entire work. LG, YS and YF confirm the authenticity of all the raw data. All authors read and approved the final version of the manuscript.

Ethics approval and consent to participate

The present study was approved by the Ethical Review Committee for Laboratory Animal Welfare of The First Hospital of Shanxi Medical University (approval no. DWLL-2024-015). All methods were performed in accordance with the relevant guidelines and regulations.

Patient consent for publication

Not applicable.

Competing interests

The authors declare that they have no competing interests.

References

1. Zhang Y, Lan F and Zhang L: Update on pathomechanisms and treatments in allergic rhinitis. Allergy 77: 3309-3319, 2022.
2. Zhang Y, Lan F and Zhang L: Advances and highlights in allergic rhinitis. Allergy 76: 3383-3389, 2021.
3. Yang T, Wang HR, Mou YK, Liu WC, Wang Y, Song XY, Ren C and Song XC: Mutual influence between allergic rhinitis and sleep: Factors, mechanisms, and interventions-a narrative review. Nat Sci Sleep 16: 1451-1467, 2024.
4. Mou YK, Wang HR, Zhang WB, Zhang Y, Ren C and Song XC: Allergic rhinitis and depression: Profile and proposal. Front Psychiatry 12: 820497, 2022.
5. Bousquet J, Schunemann HJ, Togias A, Bachert C, Erhola M, Hellings PW, Klimek L, Pfaar O, Wallace D, Ansotegui I, *et al*: Next-generation allergic rhinitis and its impact on asthma (ARIA) guidelines for allergic rhinitis based on grading of recommendations assessment, development and evaluation (GRADE) and real-world evidence. J Allergy Clin Immunol 145: 70-80.e3, 2020.
6. Shamji MH, Sharif H, Layhadi JA, Zhu R, Kishore U and Renz H: Diverse immune mechanisms of allergen immunotherapy for allergic rhinitis with and without asthma. J Allergy Clin Immunol 149: 791-801, 2022.
7. Kaczynska A, Klosinska M, Chmiel P, Janeczek K and Emeryk A: The crosstalk between the gut microbiota composition and the clinical course of allergic rhinitis: The Use of probiotics, prebiotics and bacterial lysates in the treatment of allergic rhinitis. Nutrients 14: 4328, 2022.
8. Hu Y, Zhang R, Li J, Wang H, Wang M, Ren Q, Fang Y and Tian L: Association between gut and nasal microbiota and allergic rhinitis: A systematic review. J Asthma Allergy 17: 633-651, 2024.
9. Cheng HY, Chan J, Yap GC, Huang CH, Kioh DYQ, Tham EH, Loo EXL, Shek LPC, Karnani N, Goh A, *et al*: Evaluation of stool short chain fatty acids profiles in the first year of life with childhood atopy-related outcomes. Front Allergy 3: 873168, 2022.
10. Konopelski P and Mogilnicka I: Biological effects of indole-3-propionic acid, a gut microbiota-derived metabolite, and its precursor tryptophan in mammals' health and disease. Int J Mol Sci 23: 1222, 2022.
11. Gao Y, Liu KY, Xiao W, Xie X, Liang Q, Tu Z, Yang L, Yu H, Guo H, Huang S, *et al*: Aryl hydrocarbon receptor confers protection against macrophage pyroptosis and intestinal inflammation through regulating polyamine biosynthesis. Theranostics 14: 4218-4239, 2024.
12. Zhuang H, Ren X, Jiang F and Zhou P: Indole-3-propionic acid alleviates chondrocytes inflammation and osteoarthritis via the AhR/NF-κB axis. Mol Med 29: 17, 2023.
13. Owumi SE, Najophe ES and Otunla MT: 3-Indolepropionic acid prevented chlorpyrifos-induced hepatorenal toxicities in rats by improving anti-inflammatory, antioxidant, and pro-apoptotic responses and abating DNA damage. Environ Sci Pollut Res Int 29: 74377-74393, 2022.
14. Zhou CJ, Xie BL, Han HY, Wang Y, Wang YH, Hong JY, Wei YX, Liu ZG, Feng Y, Yang G and Yang PC: Short-Chain fatty acids promote immunotherapy by modulating immune regulatory property in B cells. J Immunol Res 2021: 2684361, 2021.
15. Manning BD and Toker A: AKT/PKB signaling: Navigating the network. Cell 169: 381-405, 2017.
16. Martin LJ and Nguyen HT: Basic leucine zipper transcription factors as important regulators of leydig cells' functions. Int J Mol Sci 23: 12887, 2022.
17. Ramji DP and Foka P: CCAAT/enhancer-binding proteins: Structure, function and regulation. Biochem J 365: 561-575, 2002.
18. Hernandez-Encinas E, Aguilar-Morante D, Cortes-Canteli M, Morales-Garcia JA, Gine E, Santos A and Perez-Castillo A: CCAAT/enhancer binding protein β directly regulates the expression of the complement component 3 gene in neural cells: Implications for the pro-inflammatory effects of this transcription factor. J Neuroinflammation 12: 14, 2015.
19. Cao Y, Fan M, Pei Y, Su L, Xiao W, Chen F, Huang J, Liu X, Gu Z, Zhang Z, *et al*: CCAAT/enhancer-binding protein homologous protein (CHOP) deficiency attenuates heatstroke-induced intestinal injury. Inflammation 45: 695-711, 2022.
20. Niehrs C and Calkhoven CF: Emerging Role of C/EBPβ and epigenetic DNA methylation in ageing. Trends Genet 36: 71-80, 2020.
21. Greene LA, Zhou Q, Siegelin MD and Angelastro JM: Targeting transcription factors ATF5, CEBPB and CEBPD with cell-penetrating peptides to treat brain and other cancers. Cells 12: 581, 2023.
22. Larabee JL, Hauck G and Ballard JD: Unique, intersecting, and overlapping roles of C/EBP β and CREB in cells of the innate immune system. Sci Rep 8: 16931, 2018.
23. Liu YW, Tseng HP, Chen LC, Chen BK and Chang WC: Functional cooperation of simian virus 40 promoter factor 1 and CCAAT/enhancer-binding protein beta and delta in lipopolysaccharide-induced gene activation of IL-10 in mouse macrophages. J Immunol 171: 821-828, 2003.
24. Selter F, Hetzel T, Kahrass H and Mertz M: Animal research ethics as interaction of research ethics, animal ethics, and (animal protection) law. ALTEX 40: 541-544, 2023.
25. Shi Z, Jiang W, Chen X, Xu M, Wang J, Lai Y and Zha D: Chlorogenic acid ameliorated allergic rhinitis-related symptoms in mice by regulating Th17 cells. Biosci Rep 40: BSR20201643, 2020.
26. Bui TT, Kwon DA, Choi DW, Jung SY, Lee SY, Piao CH, Hyeon E, Fan Y, Yeon SH, Son RH, *et al*: Rosae multiflorae fructus extract and its four active components alleviate ovalbumin-induced allergic inflammatory responses via regulation of Th1/Th2 imbalance in BALB/c rhinitis mice. Phytomedicine 55: 238-248, 2019.
27. Zhang J, Gao L, Yu D, Song Y, Zhao Y and Feng Y: Three Artemisia pollens trigger the onset of allergic rhinitis via TLR4/MyD88 signaling pathway. Mol Biol Rep 51: 319, 2024.
28. Livak KJ and Schmittgen TD: Analysis of relative gene expression data using real-time quantitative PCR and the 2(-Delta Delta C(T)) Method. Methods 25: 402-408, 2001.
29. Wise SK, Damask C, Roland LT, Ebert C, Levy JM, Lin S, Luong A, Rodriguez K, Sedaghat AR, Toskala E, *et al*: International consensus statement on allergy and rhinology: Allergic rhinitis- 2023. Int Forum Allergy Rhinol 13: 293-859, 2023.
30. Goetzl EJ: Th2 cells in rapid immune responses and protective avoidance reactions. FASEB J 38: e23485, 2024.
31. Casaro M, Souza VR, Oliveira FA and Ferreira CM: OVA-induced allergic airway inflammation mouse model. Methods Mol Biol 1916: 297-301, 2019.
32. Xiao H, Tang AZ, Xu ML, Chen HL, Wang F and Li CQ: Mycobacterium vaccae attenuates airway inflammation by inhibiting autophagy and activating PI3K/Akt signaling pathway in OVA-induced allergic airway inflammation mouse model. Mol Immunol 173: 30-39, 2024.
33. Tan JK, Macia L and Mackay CR: Dietary fiber and SCFAs in the regulation of mucosal immunity. J Allergy Clin Immunol 151: 361-370, 2023.
34. Li L, Yang C, Jia M, Wang Y, Zhao Y, Li Q, Gong J, He Y, Xu K, Liu X, *et al*: Synbiotic therapy with Clostridium sporogenes and xylan promotes gut-derived indole-3-propionic acid and improves cognitive impairments in an Alzheimer's disease mouse model. Food Funct 15: 7865-7882, 2024.
35. Xu H, Luo Y, An Y and Wu X: The mechanism of action of indole-3-propionic acid on bone metabolism. Food Funct 16: 406-421, 2025.
36. Yang C, Du Y, Li Q, Liu L, Zhao L, Gao C, Tang Z, Zhang X, Zhao Y and Yang X: Fructo-oligosaccharides alleviated ulcerative colitis via gut microbiota-dependent tryptophan metabolism in association with aromatic hydrocarbon receptor activation in mice. J Agric Food Chem 72: 27912-27922, 2024.
37. Wang A, Guan C, Wang T, Mu G and Tuo Y: Lactobacillus-derived indole derivatives ameliorate intestinal barrier damage in rat pups with complementary food administration. Food Funct 15: 8775-8787, 2024.
38. Chen Y, Li Y, Li X, Fang Q, Li F, Chen S and Chen W: Indole-3-propionic acid alleviates intestinal epithelial cell injury via regulation of the TLR4/NF-κB pathway to improve intestinal barrier function. Mol Med Rep 30: 189, 2024.
39. Li G, Lin J, Zhang C, Gao H, Lu H, Gao X, Zhu R, Li Z, Li M and Liu Z: Microbiota metabolite butyrate constrains neutrophil functions and ameliorates mucosal inflammation in inflammatory bowel disease. Gut Microbes 13: 1968257, 2021.
40. Hezaveh K, Shinde RS, Klotgen A, Halaby MJ, Lamorte S, Ciudad MT, Quevedo R, Neufeld L, Liu ZQ, Jin R, *et al*: Tryptophan-derived microbial metabolites activate the aryl hydrocarbon receptor in tumor-associated macrophages to suppress anti-tumor immunity. Immunity 55: 324-340. e8, 2022.

41. York AG, Skadow MH, Oh J, Qu R, Zhou QD, Hsieh WY, Mowel WK, Brewer JR, Kaffe E, Williams KJ, *et al*: IL-10 constrains sphingolipid metabolism to limit inflammation. Nature 627: 628-635, 2024.
42. Fan K, Jin L and Yu S: Roles of regulatory B cells in the pathogenesis of allergic rhinitis. Allergol Immunopathol (Madr) 50: 7-15, 2022.
43. Fang D and Zhu J: Molecular switches for regulating the differentiation of inflammatory and IL-10-producing anti-inflammatory T-helper cells. Cell Mol Life Sci 77: 289-303, 2020.
44. Coomes SM, Kannan Y, Pelly VS, Entwistle LJ, Guidi R, Perez-Lloret J, Nikolov N, Müller W and Wilson MS: CD4(+) Th2 cells are directly regulated by IL-10 during allergic airway inflammation. Mucosal Immunol 10: 150-161, 2017.
45. Mitchell RE, Hassan M, Burton BR, Britton G, Hill EV, Verhagen J and Wraith DC: IL-4 enhances IL-10 production in Th1 cells: Implications for Th1 and Th2 regulation. Sci Rep 7: 11315, 2017.
46. Caucheteux SM, Hu-Li J, Guo L, Bhattacharyya N, Crank M, Collins MT and Paul WE: IL-1β enhances inflammatory TH2 differentiation. J Allergy Clin Immunol 138: 898-901.e4, 2016.
47. van der Krieken SE, Popeijus HE, Mensink RP and Plat J: CCAAT/enhancer binding protein β in relation to ER stress, inflammation, and metabolic disturbances. Biomed Res Int 2015: 324815, 2015.
48. Zhou J, Li H, Xia X, Herrera A, Pollock N, Reebye V, Sodergren MH, Dorman S, Littman BH, Doogan D, *et al*: Anti-inflammatory activity of MTL-CEBPA, a small activating RNA drug, in LPS-stimulated monocytes and humanized mice. Mol Ther 27: 999-1016, 2019.
49. Collins CB, Puthoor PR, Nguyen TT, Strassheim D, Jedlicka P, Friedman JE and de Zoeten EF: C/EBPβ deletion promotes expansion of poorly functional intestinal regulatory T cells. J Crohns Colitis 12: 1475-1485, 2018.
50. Liu Q, Peng Z, Zhou L, Peng R, Li X, Zuo W, Gou J, Zhou F, Yu S, Huang M and Liu H: Short-chain fatty acid decreases the expression of CEBPB to inhibit mir-145-mediated DUSP6 and thus further suppresses intestinal inflammation. Inflammation 45: 372-386, 2022.
51. Weichhart T, Hengstschlager M and Linke M: Regulation of innate immune cell function by mTOR. Nat Rev Immunol 15: 599-614, 2015.
52. Xu J, Ye Y, Ji J, Sun J, Wang JS and Sun X: Untargeted metabolomic profiling reveals changes in gut microbiota and mechanisms of its regulation of allergy in OVA-Sensitive BALB/c mice. J Agric Food Chem 70: 3344-3356, 2022.
53. Tang Y, She Y, Chen D, Zhou Y, Xie D and Liu Z: 16S rRNA sequencing-based evaluation of the protective effects of key gut microbiota on inhaled allergen-induced allergic rhinitis. Front Microbiol 15: 1497262, 2024.